Diabetes, Metabolic Syndrome and Obesity Dovepress

Open Access Full Text Article ORIGINAL RESEARCH

White Matter Function and Network Abnormalities in Patients with Diabetic Retinopathy

Yu-Lin Zhong[1,*], Rui-Yang Hu[2,*], Yuan-Zhi He[3], Xiao-Tong Li[3], Zi-Cong Li[4], Xin Huang[1]

[1]Department of Ophthalmology, Jiangxi Provincial People's Hospital, The First Affiliated Hospital of Nanchang Medical College, Nanchang, Jiangxi, 330006, People's Republic of China; [2]School of Ophthalmology and Optometry, Jiangxi Medical College, Nanchang University, Nanchang, Jiangxi, 330006, People's Republic of China; [3]Queen Mary School, Jiangxi Medical College, Nanchang University, Nanchang, Jiangxi, 330006, People's Republic of China; [4]Department of Radiology, Jiangxi Provincial People's Hospital, The First Affiliated Hospital of Nanchang Medical College, Nanchang, Jiangxi, 330006, People's Republic of China

*These authors contributed equally to this work

Correspondence: Zi-Cong Li, Department of radiology, Jiangxi Provincial People's Hospital, No. 152, Ai Guo Road, Dong Hu District, Nanchang, Jiangxi, 330006, People's Republic of China, Email 39652858@qq.com; Xin Huang, Department of ophthalmology, Jiangxi Provincial People's Hospital, No. 152, Ai Guo Road, Dong Hu District, Nanchang, Jiangxi, 330006, People's Republic of China, Tel +86 15879215294, Email 334966891@qq.com

Background: This study aims to explore changes in white matter function and network connectivity in individuals with DR.

Methods: This study included 46 patients with DR and 43 age- and gender-matched healthy control (HC) participants were enrolled in the study. The aim was to investigate inter-group differences in white matter (WM) function and to analyze changes in the WM network among DR patients.

Results: Increased degree centrality (DC) values were observed in the middle cerebellar peduncle and genu of the corpus callosum, while higher fractional amplitude of low-frequency fluctuations (fALFF) values were found in the left superior corona radiata, right anterior corona radiata, and right superior longitudinal fasciculus. Conversely, reduced regional homogeneity (ReHo) values were noted in the left posterior thalamic radiation among patients with DR compared to HC, with statistical correction applied The SVM classification accuracy for distinguishing between DR and HC patients based on WM measures indicated values of 81.52%, 80.43%, and 89.13% for DC, fALFF, and ReHo, respectively, with respective area under the curve (AUC) values of 0.87, 0.85, and 0.93. Furthermore, alterations were detected within specific brain regions including the body of corpus callosum (BCC), splenium of corpus callosum (SCC), genu of corpus callosum (GCC), left posterior thalamic radiation (PTR), right anterior corona radiata (ACR), and right posterior corona radiata (PCR) in the DR group compared to HCs, with an intra-network decrease in connectivity. Interestingly, the left superior longitudinal fasciculus (SLF) within the DR group exhibited an intra-network increase compared to the HC group.

Conclusion: DR exhibited abnormal white matter functional alterations, particularly affecting the fiber pathways linking the visual network to the sensory-motor network.

Keywords: diabetic retinopathy, degree centrality, DC, fractional amplitude of low-frequency fluctuation, fALFF, regional homogeneity, ReHo, independent component analysis, ICA

Introduction

Diabetic retinopathy (DR) is the predominant microvascular complication in individuals with diabetes and a significant contributor to vision loss in this population. The hallmark progression of DR involves transitions from microaneurysms to exudative lesions, subsequently resulting in macular edema, ischemia, cotton wool spots, microvascular abnormalities, vein beading, and proliferative alterations.[1,2] As of March 2020, the global prevalence of DR was 22.27%. It is projected to escalate to 103.12 million in 2020, 130 million in 2030, and 165 million in 2045, with the highest prevalence recorded in Africa (35.90%) and North America (33.30%), and the lowest in Central and South America (13.37%).[3,4] The rising occurrence of DR annually is linked to factors like aging populations and environmental shifts. Studies have revealed

Received: 19 August 2024
Accepted: 24 October 2024
Published: 3 November 2024

a notable heightened risk of cognitive decline, dementia, and Alzheimer's disease among individuals with DR, likely due to brain structural and functional modifications in these patients.[5,6] Furthermore, pathological transformations including neuroinflammation, vascular degeneration, and neuroglial activation are evident in both DR and Alzheimer's disease.[7] Of these, aberrant microglial-vascular function may contribute to early vascular impairment in DR.[8] In addition, the presence of altered retinal vascular density in DR patients may also be one of the potential markers of cerebrovascular injury in DR patients.[9] Examining the abnormal brain function in DR patients could offer insights into detecting neuroimaging variations in this population in the future.

Prior neuroimaging investigations in individuals with DR have primarily centered on gray matter structure and function. Studies involving both type 1 and type 2 diabetes mellitus have revealed variations in surface area, cortical thickness, gray matter density, and volume.[10–13] Patients with diabetes, with or without microangiopathy, displayed disparate degrees of gray matter volume reduction, particularly in sensorimotor and vision-related regions.[14–16] Noteworthy abnormalities in gray matter function within the occipital lobe and vision-related regions were also observed in individuals with DR. Furthermore, patients with DR exhibited irregular gray matter function in sensorimotor and visually associated areas. The amplitude of low-frequency fluctuations (ALFF) in regions like the occipital lobe, cuneate lobe, talar fissure, cerebellum, and hippocampus, pertaining to vision and sensorimotor functions, showed distinct alterations in DR patients.[17–19] Regional homogeneity (ReHo), degree centrality (DC), and functional connection strength (FCS) values in DR patients were concentrated in these identified regions as well. However, these studies have predominantly scrutinized gray matter anomalies, overlooking potential aberrations in the white matter (WM), a vital component of the brain.[20–22] While these studies have primarily emphasized the abnormal alterations in the brain's gray matter, they have overlooked the abnormal changes occurring in the white matter (WM), a crucial element of the brain.

Recent studies have demonstrated the reliable detection of Blood Oxygenation Level-Dependent (BOLD) signals in WM, with these signals encoding neural activity through varying degrees of correlation in intensity and time delay. Huang et al showcased that traditional fMRI methods can detect BOLD signals in the WM, with changes modulated by neural activity.[23] Li et al identified a weak small-world topology and nonrandom patterns in the WM functional connectome, offering preliminary support for utilizing the WM connectome.[24] Subsequently, peer et al verified that the identified WM BOLD signals form functional networks,[25] paving the way for investigating the link between white matter functional networks and clinical diseases. Exploration of WM function and deviations in the WM network has been explored across various conditions like Alzheimer's disease,[26] Parkinson's disease,[27] and early blindness.[28] Past research has revealed diverse white matter microstructural changes in both type 1 and type 2 diabetes mellitus.[29,30] In a study of patients with proliferative diabetic retinopathy, hyperintensities were observed in the white matter volume of the bilateral lentiform nuclei, indicating structural anomalies in the WM.[31] This establishes the foundation for the current study, which aims to determine whether individuals with DR exhibit WM functional abnormalities and network deviations.

Numerous fMRI techniques exist for assessing local neural activity and alterations in brain networks. DC can reveal the connectivity of brain networks at the voxel level by indicating nodes connected to regions with higher centrality values; thus, higher DC values signify greater centrality or importance within the functional network.[32] The fractional amplitude of low-frequency fluctuations (fALFF) serves as a bioindicator capable of capturing neural activity spontaneously while being less susceptible to motion artifacts.[33] Unlike the localized activity measure ALFF, fALFF is less influenced by physiological noise during imaging.[34,35] The regional homogeneity (ReHo) method assesses coherence in blood oxygen level-dependent signals among neighboring voxels across the entire brain during rest.[36,37] ReHo is a primary method used to study local synchronization of spontaneous fMRI signals, specifically designed to evaluate regional resting-state brain activity. Independent Component Analysis (ICA) is widely employed for blind source separation in medical imaging, effectively identifying and characterizing functional networks from rs-fMRI data. ICA has been instrumental in investigating various clinical disorders associated with alterations in brain networks.[38–40]

The preceding research has revealed significant changes in brain function and white matter structure among individuals with diabetic retinopathy. Nonetheless, the influence of diabetic retinopathy on white matter function in the brain remains ambiguous, including the presence of a distinct pattern of damage. Our hypothesis suggests that patients with diabetic retinopathy exhibit abnormal modifications in white matter function and connectivity. To achieve

this objective, 46 DR patients and 43 healthy control (HC) individuals were selected and partitioned into two groups under the assumption of distinctive changes in white matter function and network in DR patients. The analysis included assessing brain white matter function utilizing resting-state fMRI metrics of DC, fALFF, and ReHoacross all participants. Subsequently, a SVM algorithm was employed to determine if alterations in white matter DC, fALFF, and ReHo could effectively discriminate between DR patients and HC individuals. Furthermore, the intra- and inter-network connectivity within subjects' cerebral white matter networks was investigated separately employing ICA methodology.

Methods

Participants

All participants consented in writing to partake in the study. A total of 46 DR patients, comprising 22 males and 24 females, were recruited from the Department of Ophthalmology at Jiangxi Provincial People's Hospital. The diagnostic criteria for DR patients included fasting plasma glucose levels ≥ 7.0 mmol/L, random plasma glucose levels ≥ 11.1 mmol/L, or a 2-hour glucose level ≥ 11.1 mmol/L. Furthermore, patients with nonproliferative DR exhibited characteristics such as microaneurysms, hard exudates, and retinal hemorrhages.

The exclusion criteria for DR patients encompassed proliferative DR with retinal detachment, vitreous hemorrhage, other ocular-related complications (such as cataract, glaucoma, high myopia, or optic neuritis), and the coexistence of diabetic nephropathy or neuropathy.

All healthy controls (HCs) met the criteria, which comprised fasting plasma glucose levels < 7.0 mmol/L, random plasma glucose levels < 11.1 mmol/L, HbA1c levels < 6.5%, absence of ocular diseases (myopia, cataracts, glaucoma, optic neuritis, or retinal degeneration), binocular visual acuity ≥ 1.0 (decimal), no history of ocular surgery, and no mental disorders. More comprehensive details about the participants are elaborated in the study.

Statement of Ethics

The study adhered to the principles outlined in the Declaration of Helsinki and obtained approval from the Ethics Committee of Jiangxi Provincial People's Hospital. Prior to enrollment, all participants provided written informed consent.

MRI Acquisition

MRI imaging was conducted using a 3-T MR scanner (Discovery 750W System; GE Healthcare, Chicago, IL, United States) equipped with an 8-channel head coil. To minimize head movements, foam pads were positioned on both sides of the jaw, and earplugs were utilized to reduce ambient noise throughout the scanning procedure. Participants were instructed to close their eyes, relax, minimize movements, maintain mental clarity, and remain awake during the scan. Whole-brain T1 weights were obtained with three-dimensional brain volume imaging (3D-BRAVO) MRI with the following parameters: repetition time (TR)/echo time (TE) = 8.5/3.3, thickness = 1.0 mm, no intersection gap, acquisition matrix = 256 × 256, field of view = 240×240 mm2, and flip angle = 12°. Functional images were obtained by using a gradient echoplanar imaging sequence with the following parameters: TR/TE = 2000 ms/25 ms, thickness = 3.0 mm, gap = 1.2 mm, acquisition matrix = 64 × 64, flip angle = 90°, field of view = 240×240 mm2, voxel size = 3.6×3.6 × 3.6 mm3, and 35 axial slices. All the subjects were instructed to rest quietly with their eyes closed and relaxed without thinking about anything in particular or falling asleep.

fMRI Data Processing

The rs-fMRI data underwent preprocessing utilizing the Data Processing & Analysis of Brain Imaging (DPABI) toolbox and Statistical Parametric Mapping 12 (SPM12) within MATLAB (2018b). The preprocessing involved several key steps: 1) converting original DICOM-format files to the NIfTI format, discarding the initial 10 time points per subject to stabilize the signal and acclimate participants to scanning noise, conducting slice-timing and motion correction, 2) segmenting T1 images into gray matter (GM), white matter (WM), and cerebrospinal fluid (CSF) and aligning them with the mean BOLD image, eliminating linear trends and regressing noise signals—with

an exclusive focus on head motion and CSF averages to retain relevant signals. 3)Individual-level WM 4D images were extracted by categorizing each voxel as GM, WM, or CSF based on T1 image segmentation, followed by spatial smoothing (FWHM = 4 mm) on WM and GM images per subject. Group-level WM masks were created using voxels identified as WM in >90% of the subjects, excluding subcortical regions per the Harvard-Oxford Atlas. 4) The WM mask was coregistered with the functional space, resampled to process the functional image.

DC of WM Calculation

DC data analysis involves assessing at the voxel level using DPABI software. A Pearson correlation coefficient matrix was created by calculating temporal correlations between a white matter (WM) mask voxel and all other brain voxels. To mitigate interference from low temporal correlations due to signal noise, a threshold of $r > 0.25$ was applied to the Pearson correlation coefficient. Subsequently, Fisher-z transformation was applied to convert the voxel-wise DC values into a z-score graph to improve normality.

fALFF of WM Calculation

The fALFF was computed using the DPABI Data Analysis Toolkit. For each voxel, the power spectrum was obtained by converting the smoothed signal from the time domain to the frequency domain utilizing fast Fourier transform (FFT). Subsequently, the square root of the power spectrum at each frequency in the 0.01 to 0.15 hz range was determined, resulting in the average square root for each voxel. The fALFF value for each voxel was then normalized by dividing it by the average fALFF value. This normalization ratio helps diminish the individual differences in global effects, as the fALFF value represents the ratio of the ALFF value within the specified frequency band (eg, 0.01–0.15 hz) to the total ALFF across all frequency bands.

ReHo of WM Calculation

The ReHo map was created through the calculation of Kendall's coefficient of concordance (KCC) between the time series of a voxel and its nearest neighbor (26 voxels) on a voxel-wise basis. The computation of the KCC value has been elucidated in a prior research.[36] To standardize the results, the ReHo value of each voxel was normalized by the average ReHo across the individual's brain. Following the ReHo computation, spatial smoothing with a full width at half maximum (FWHM) of 6 mm was conducted.

Support Vector Machine Analysis

We employed machine learning analyses with the Support Vector Machine (SVM) algorithm to assess the potential diagnostic utility of DC, fALFF, and ReHo maps in DR and HC group. Using the Pattern Recognition for Neuroimaging Toolbox,[41] the DC, fALFF, and ReHo values of distinctive brain regions among groups were utilized as classification features. Leave-one-out cross-validation (LOOCV) was implemented to validate the SVM classifier, with accuracy, sensitivity, and specificity serving as performance metrics. Receiver operating characteristic (ROC) curves and their corresponding areas under the curve (AUCs) were generated to evaluate classification effectiveness.

Group Independent Component Analysis

Group ICA was conducted to decompose the data into independent components (ICs) using the GIFT toolbox (version 3.0a). Following voxel-wise demeaning and variance normalization, white matter (WM) images in standard space were included in the analysis. Subsequently, the 4D fMRI data from individual participants were merged into a single dataset and decomposed into spatial and temporal domains. Notably, the mean of the time series was retained in the fMRI data processing. We designated 20 as the number of independent components and set the threshold for the component spatial maps at $P < 1.0$. Eight independent components were chosen out of the 20 based on the alignment of their spatial maps' time course with the stimulus signal waveform.[42]

Functional Network Connectivity

The Functional Network Connectivity (FNC) analysis was conducted utilizing the MANCOVAN toolbox within the GIFT software to investigate alterations in the predefined 8 spatial independent component pairs implicated in functional

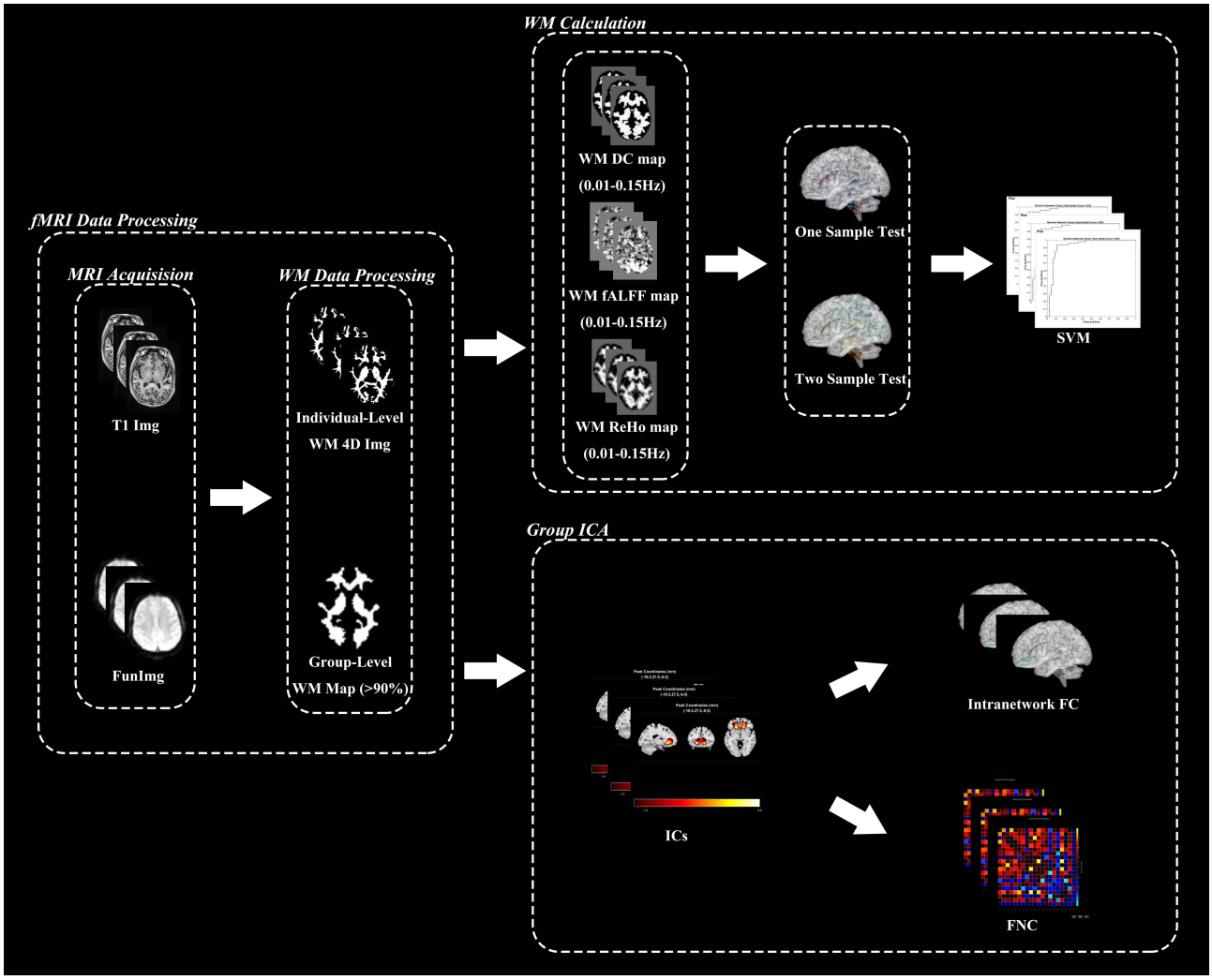

Figure 1 This flowchart outlines the preprocessing, statistical analysis, and machine learning procedures conducted in this study. Initially, functional and structural brain images of the subjects were extracted separately. Subsequently, white matter functional images were computed, with preservation of over 90% of them for the creation of white matter templates. Following this, one-sample and two-sample tests for Degree Centrality (DC), fractional Amplitude of Low-Frequency Fluctuations (fALFF), and Regional Homogeneity (ReHo) in diabetic retinopathy (DR) and healthy control (HC) groups were performed based on the white matter template. Machine learning techniques were then applied. In parallel, the smoothed white matter images underwent independent component analysis (ICA). An initial selection of 20 independent components was made, with 8 components chosen for further analysis. The remaining independent components underwent intra- and inter-network evaluations.
Abbreviations: WM, white matter; DR, diabetic retinopathy; HC, healthy control; DC, degree centrality; fALFF, fractional amplitude of low-frequency fluctuations; ReHo, regional homogeneity; ICA, independent component analysis; IC, independent component; FNC, functional network connectivity.

connections. Initially, at the 0.01–0.15 hz range, preprocessing steps including detrending, depeaking, and low-pass filtering were applied to the selected independent components (ICs). Subsequently, pair-wise correlations of these ICs were computed and transformed using Fisher's Z-transform. The study flow is visually depicted in Figure 1.

Statistical Analysis

Both the chi-square ($\chi 2$) test and independent-samples *t*-test were employed to compare clinical variables between the two groups using the Statistical Package for the Social Sciences (SPSS) version 26, developed by IBM Corp., Armonk, N.Y., USA. The analysis included gender comparisons.

Differences in WM DC values, WM fALFF values, and WM ReHo values between the DR and HC groups were analyzed at the group level using two-sample t-tests. Age, sex, and head movement were accounted for as covariates in the Data Analysis Module of the DPABI Toolkit. Correction for multiple comparisons was executed through the Gaussian Random Field (GRF) method, specifying a voxel-level significance level of $P < 0.001$ (two-tailed) and

a cluster-level significance of P < 0.05. Brain regions exhibiting significant group differences in the metric analysis were delineated based on the ICBM-DTI-81 white matter label atlas (JHU DTI-based WM atlases, provided by Dr. Susumu Mori, Laboratory of Brain Anatomical MRI, Johns Hopkins University).[43,44]

Intra-network functional connectivity (FC) within resting-state network (RSN) maps was assessed using two-sample t-tests to identify differences between the two groups. Multiple comparisons were corrected for using the Gaussian random field method, with age and sex as covariates, in SPM12 software. Group comparisons were restricted to voxels within the respective RSNs, applying a significance threshold of $p < 0.01$ at the voxel-level (corrected using Gaussian random field) and $p < 0.05$ at the cluster-level.

Internetwork functional connectivity analysis was employed to determine temporal relationships among white matter bundles. Average time lags were computed for each group based on significant correlation pairs, indicating the delay between the time courses of correlated white matter bundles. Two-sample t-tests were conducted to compare unique temporal relationships between resting-state networks (RSNs) in the two groups at a significance level of $p < 0.01$ (not corrected).

Results

Demographics and Disease Characteristics

There were no significant differences in age and gender between the two groups ($p > 0.05$). Significant discrepancies in best-corrected visual acuity (BCVA) were observed between the groups ($p < 0.05$). (Table 1).

Different WM Values

In our study, one-sample t-tests were conducted to analyze the white matter signal values in patients with DR and HC group as illustrated in Figure 2. Specifically, Figure 2A presents the results of white matter DC signal values in DR patients, while Figure 2B displays the results of white matter DC signal values HC group. Additionally, Figure 2C and D show the results of white matter fALFF signal values in DR and HC group, respectively. Lastly, Figure 2E and F depict the results of white matter ReHo signal values in DR and HC group, respectively.

The results showed that compared with HC patients, white matter DC signal values were elevated in the middle cerebellar peduncle and genu of corpus callosum in DR patients compared with HC group. (Figure 3A) and the different mean DC values between two groups. (Figure 3B) The white matter fALFF values were also ascended in the left superior corona radiata, right anterior corona radiata and right superior longitudinal fasciculus in DR patients compared with HC group. (Figure 3C) and the different mean fALFF values between two groups. (Figure 3D) As for the white matter ReHo values, they were shown a decrease signal in the left posterior thalamic radiation.(Figure 3E) and the different mean ReHo values between two groups.(Figure 3F) (corrected for GRF, voxel-level P < 0.001, cluster-level P < 0.05; Table 2).

Table 1 Clinical-Demographic Characteristics of the DR and HC Groups

Condition	DR Group	HC Group	t	p
Gender (male/female)	22/24	22/21	N/A	N/A
Age (years)	55.16 ± 1.43	53.17± 2.13	−0.215-3.-2.561	0.74
BCVA-OD	0.42 ± 0.17	1.12± 0.15	2.561	0.001*
BCVA-OS	0.31± 0.215	1.12 ± 0.13	−3.132	0.001*
HbA1c (%)	7.48±0.63	N/A	N/A	N/A
Fasting blood glucose (mmol/L)	8.04±0.92	N/A	N/A	N/A

Notes: $\chi 2$ test for sex (n). Independent *t* test for the other normally distributed continuous data (means ± SD). "*"indicate P<0.001.

Abbreviations: DR, diabetic retinopathy; HC, healthy control; N/A, not applicable; BCVA, best corrected visual acuity; OD, oculus Dexter; OS, oculus sinister; DR, diabetic retinopathy; HC, healthy controls.

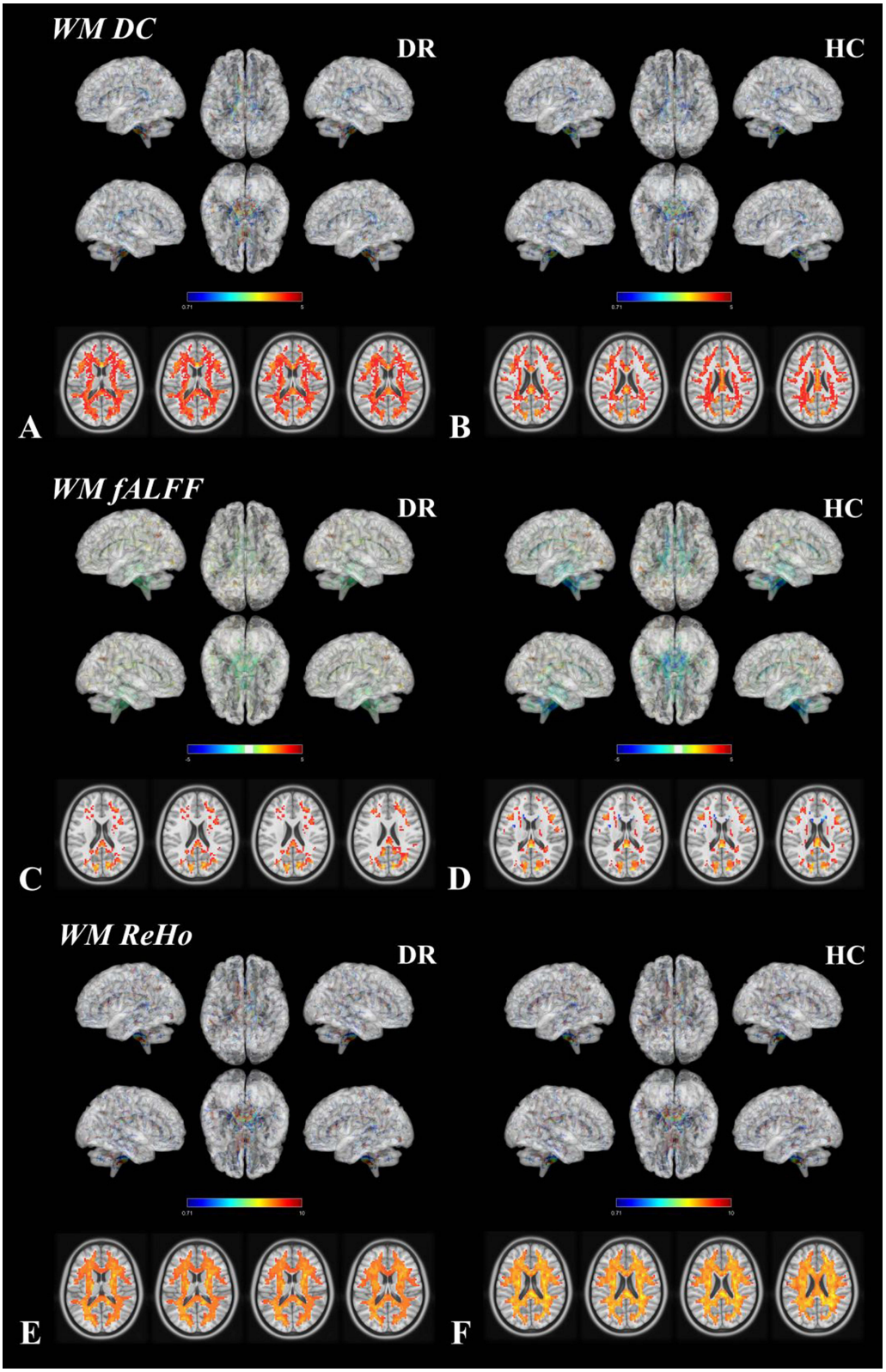

Figure 2 Results of one-sample t-tests for white matter DC signal values, white matter fALFF signal values and white matter ReHo signal values in DR and HC. (**A**) Results of white matter DC signal values in DR patients. (**B**) White matter DC signal value results in HC group. (**C**) Results of white matter fALFF signal values in DR patients. (**D**) Results of white matter fALFF signal values in HC group. (**E**) Results of white matter ReHo signal values in DR patients. (**F**) Results of white matter ReHo signal values in HC group.

Abbreviations: DR, diabetic retinopathy; HC, healthy control; DC, degree centrality; fALFF, fractional amplitude of low-frequency fluctuations; ReHo, regional homogeneity.

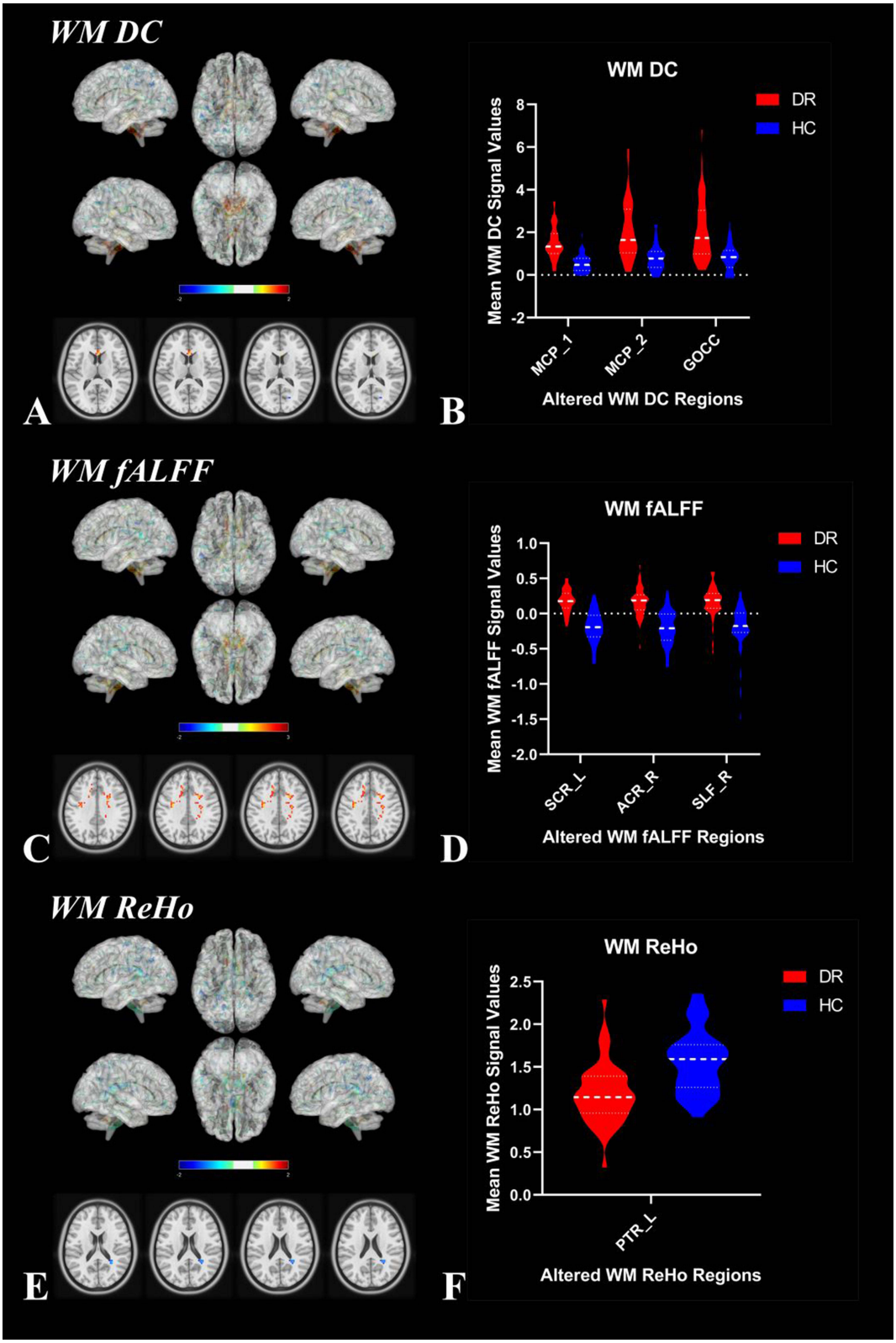

Figure 3 Two-sample *t*-test results of white matter DC signal values, white matter fALFF signal values and white matter ReHo signal values in DR patients and HC group. (**A** and **B**) Results of the white matter DC values. (**C** and **D**) Results of the white matter fALFF values. (**E** and **F**) Results of the white matter ReHo values.
Abbreviations: DR, diabetic retinopathy; HC, healthy control; DC, degree centrality; fALFF, fractional amplitude of low-frequency fluctuations; ReHo, regional homogeneity; MCP, middle cerebellar peduncle; GOCC, genu of corpus callosum; SCR_L, left superior corona radiata; ACR_R, right anterior corona radiata; SLF_R, right superior longitudinal fasciculus; PTR_L, left posterior thalamic radiation.

Table 2 White Matter Areas Showing Abnormal Signal Values in DR Patients

Metrics	Tract (JHU-Atlas)	Voxels	MNI Coordinates			t-Values
			x	y	z	
DC	Middle_cerebellar_peduncle_1	50	−12	−36	−39	5.39017
	Middle_cerebellar_peduncle_2	32	3	−15	−27	5.3554
	Genu_of_corpus_callosum	21	3	21	12	5.84174
fALFF	Superior_corona_radiata_L	239	15	−15	48	5.64146
	Anterior_corona_radiata_R	102	−18	24	24	5.36133
	Superior_longitudinal_fasciculus_R	29	−33	−12	36	5.49762
ReHo	Posterior_thalamic_radiation_L	22	30	−48	15	−5.03146

Notes: (The statistical threshold was set at voxel with P < 0.001 and cluster with P < 0.05 for GRF correction.).
Abbreviations: DR, diabetic retinopathy; HC, healthy control; DC, degree centrality; fALFF, fractional amplitude of low-frequency fluctuations; ReHo, regional homogeneity.

Support Vector Machine Results

The SVM classification based on WM DC values reaches a total accuracy of 81.52% and the ROC curve of the SVM classifier with an AUC value of 0.87 (Figure 4A and B). The SVM classification based on WM fALFF values reaches a total accuracy of 80.43% and the ROC curve of the SVM classifier with an AUC value of 0.85 (Figure 4C and D). The SVM classification based on WM ReHo values reaches a total accuracy of 89.13% and the ROC curve of the SVM classifier with an AUC value of 0.93 (Figure 4E and F).

Identification of Static White Matter Bundles

Typical spatial pattern maps of white matter bundles in the DR and HC groups (Figure 5), respectively, IC06(SCC, splenium of corpus callosum), IC07(UF1, uncinate fasciculus1), IC08(PTR, posterior thalamic radiation), IC10(ACR1, Anterior corona radiata1), IC12(ACR2, Anterior corona radiata2), IC13(ACR3, Anterior corona radiata3), IC15(UF2, uncinate fasciculus2), IC19(SLF, superior longitudinal fasciculus).

Intra- and Inter Network Functional Connectivity Changes

In the diabetic retinopathy (DR) group, there was an intra-network decrease in the body of the corpus callosum (BCC) depicted in IC06 (Figure 6A), the splenium of the corpus callosum (SCC) represented by IC08 (Figure 6B), the genu of the corpus callosum (GCC) and the left posterior thalamic radiation (PTR) shown in IC12 (Figure 6C), the right anterior corona radiata (ACR) displayed in IC13 (Figure 6D), and the right posterior corona radiata (PCR) illustrated in IC19 (Figure 6E) compared to the healthy control (HC) group. Conversely, the left superior longitudinal fasciculus (SLF) in the DR group exhibited an intra-network increase relative to the HC group.(Figure 6 and Table 3) (two-tailed, voxel-level $p < 0.01$, GRF correction, cluster-level $p < 0.05$).

The mean functional network connectivity (FNC) map is presented in Figure 7A. Significant changes and the direction of differences resulting from two-sample t-tests comparing DR and HC groups for each correlation pair are represented as -sign(t val)log10(p val). Specifically, the connections of the uncinate fasciculus (UF) with the posterior thalamic radiation (PTR) and anterior corona radiata (ACR) were identified as significantly different between the two groups ($p < 0.05$) (Figure 7B and Table 4).

Discussion

In this study, we investigated WM functionality in DR patients. First, in the DC analysis, abnormalities were observed in the middle cerebellar peduncle and genu of the corpus callosum in the DR group compared to the HC group. Second, the fALFF analysis revealed abnormalities in the left superior corona radiata, right anterior corona radiata, and right superior longitudinal fasciculus in the DR group. Notably, these regions showed increased DC and fALFF values compared to HC. Third, the ReHo analysis identified decreased activity in the left posterior thalamic radiation in the DR group.

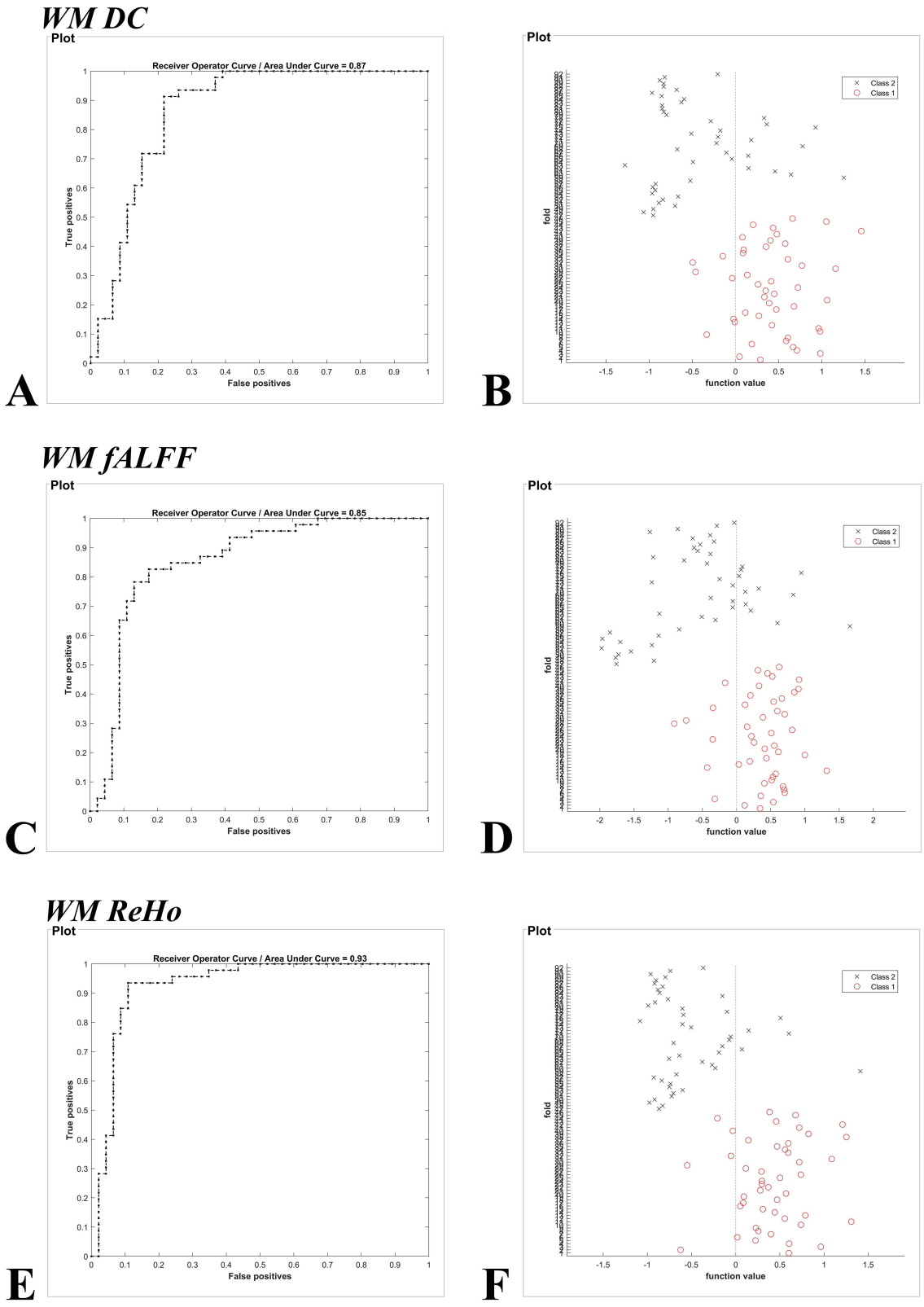

Figure 4 Machine classification results based on (**A** and **B**) white matter DC signal values, (**C** and **D**) white matter fALFF signal values and (**E** and **F**) white matter ReHo signal values. The left column shows the ROC curve of the SVM classifier with AUC values of 0.87, 0.85 and 0.93, and the right column of images shows a 10-fold in the class 1 (DR group) and class 2 (HC group), respectively.

Abbreviations: WM, white matter; SVM, support vector machine; DC, degree centrality; fALFF, fractional amplitude of low-frequency fluctuations; ReHo, regional homogeneity.

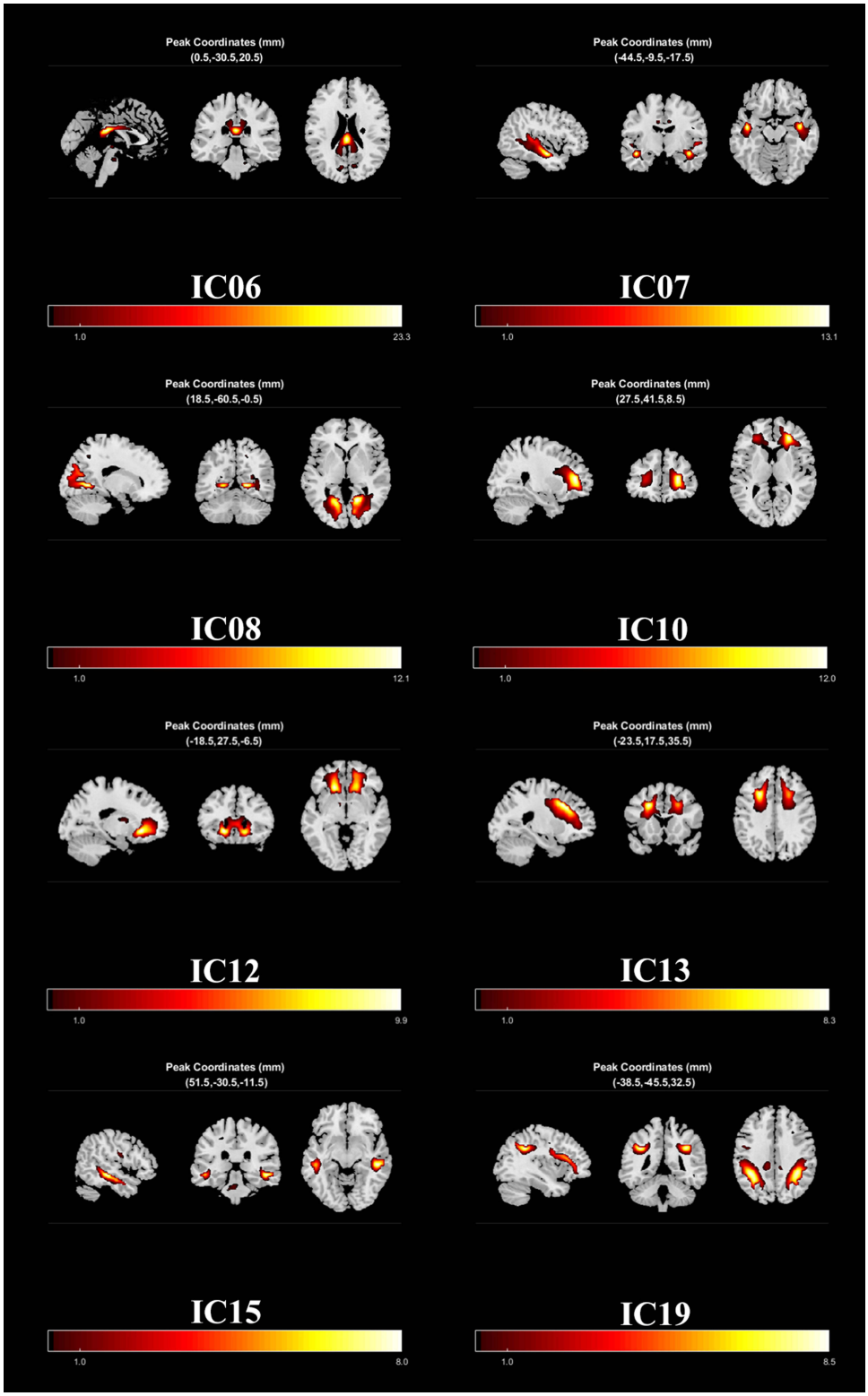

Figure 5 Classical spatial patterns for each white matter bundles in DR and HC groups, including IC06(SCC), IC07(UF1), IC08(PTR), IC10(ACR1), IC12(ACR2), IC13 (ACR3), IC15(UF2), IC19(SLF). Scale represents T-values with a range of 1–24.8 in each white matter bundles.

Abbreviations: DR, diabetic retinopathy; HC, healthy control; SCC, splenium of corpus callosum; UF, uncinate fasciculus; PTR, posterior thalamic radiation; ACR, Anterior corona radiata; SLF, superior longitudinal fasciculus.

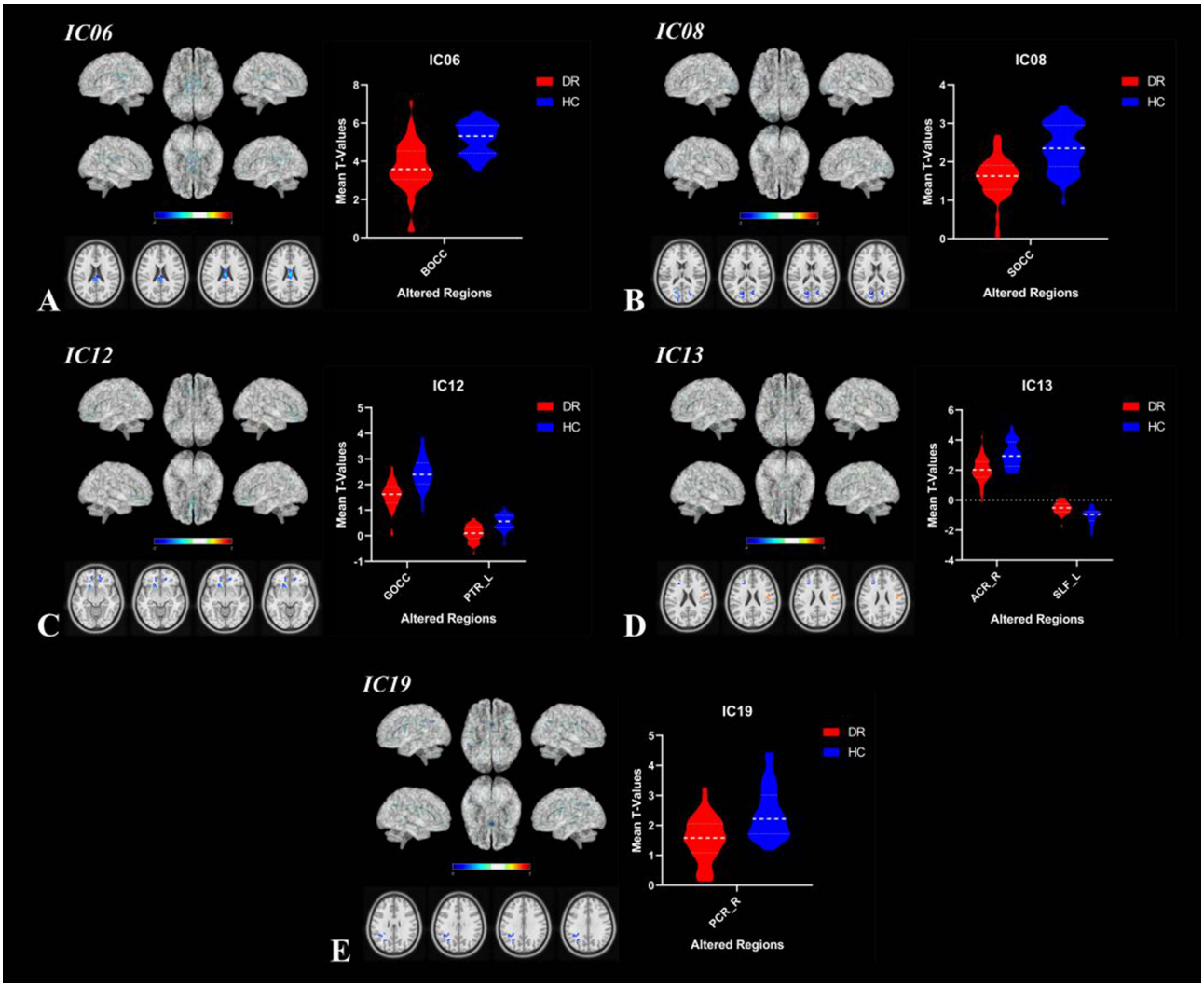

Figure 6 The DR group had differential white matter networks compared to the HC group. The warm colors indicate increased strength of functional connectivity and the cold colors indicate reduced strength of functional connectivity. In the diabetic retinopathy (DR) group, there was an intra-network decrease in the body of the corpus callosum (BCC) depicted in IC06 (**A**), the splenium of the corpus callosum (SCC) represented by IC08 (**B**), the genu of the corpus callosum (GCC) and the left posterior thalamic radiation (PTR) shown in IC12 (**C**), the right anterior Corona radiata (ACR) displayed in IC13 (**D**), and the right posterior corona radiata (PCR) illustrated in IC19 (**E**) compared to the healthy control (HC) group. Conversely, the left superior longitudinal fasciculus (SLF) in the DR group exhibited an intra-network increase relative to the HC group. (two-tailed, voxel-level $p < 0.01$, GRF correction, cluster-level $p < 0.05$).

Abbreviations: DR, diabetic retinopathy; HC, healthy control; BOCC, body of corpus callosum; SOCC, splenium of corpus callosum; GOCC, genu of corpus callosum; PTR_L, left posterior thalamic radiation; ACR_R, right anterior corona radiata; SLF_L, left superior longitudinal fasciculus; PCR_R, right posterior corona radiata.

Furthermore, classifying DR patients based on WM DC values, WM fALFF values, and WM ReHo values resulted in overall correct classification rates of 81.52%, 80.43%, and 89.13%, with area under the receiver operating characteristic (ROC) curves of 0.87, 0.85, and 0.93, respectively, offering new insights into WM functional alterations in DR patients. Lastly, independent component (IC) analysis within the network highlighted intra-network decreases in body of the corpus callosum (BCC) in IC06, splenium of the corpus callosum (SCC) in IC08, genu of the corpus callosum (GCC) and left posterior thalamic radiation (PTR) in IC12, right anterior corona radiata (ACR) in IC13, and right posterior corona radiata (PCR) in IC19 in the DR group compared to the HC group. Conversely, an intra-network increase was observed in the left superior longitudinal fasciculus (SLF) in the DR group. Additionally, the uncinate fasciculus (UF)-PTR and UF-ACR connections were found to be significant across the whole white matter network correlations in the DR group.

The middle cerebellar peduncle (MCP), also referred to as the cerebral pontine arm, serves as an afferent fiber pathway of the cerebellum, with its primary white matter bundle being the cerebral pontine cerebellar fasciculus. Originating in the pontine nucleus, this cerebellar bundle extends to the contralateral cerebellum. The superior white

Table 3 Different Intra-Network FC Between the DR and HC

ICs	Tract (JHU-Atlas)	Voxels	MNI Coordinates			t-Values
			x	y	z	
IC06	Body_of_corpus_callosum	41	0	−18	24	−4.81707
IC08	Splenium_of_corpus_callosum	88	−15	−72	15	−4.71347
IC12	Genu_of_corpus_callosum Posterior_thalamic_radiation_L	114 52	−18 27	18 −78	−9 0	−4.51904 −4.74308
IC13	Anterior_corona_radiata_R Superior_longitudinal_fasciculus_L	59 44	−24 45	21 −9	33 24	−4.78119 5.78175
IC19	Posterior_corona_radiata_R	28	−42	−48	30	−3.84126

Notes: (The statistical threshold was set at voxel with P < 0.001 and cluster with P < 0.05 for GRF correction.).
Abbreviations: DR, diabetic retinopathy; HC, healthy control; IC, independent component; FC, functional connectivity.

matter tract associated with the pontine cerebellar tract is the corticobulbar tract, responsible for receiving neural signals from various regions of the cerebral cortex, including the middle frontal gyrus, middle-inferior temporal gyrus, and occipital lobe. Furthermore, Andica et al reported a significant decrease in fiber density (FD), macrostructural fiber-fiber density (FD), macrostructural fiber cross-section (FC), and the combined FD and FC (FDC) in MCP white matter tracts of patients with Metabolic Syndrome compared to healthy controls.[45] Metabolic syndrome encompasses a cluster of interconnected risk factors for type 2 diabetes and cardiovascular disease, characterized by glucose intolerance, abdominal obesity, hypertension, and dyslipidemia. The elevated degree centrality (DC) values observed in the middle cerebellar peduncle (MCP) among patients with diabetic retinopathy (DR) in this study suggest a potential association with glucose dysregulation. Additionally, situated beneath the posterior section of the middle frontal gyrus lies the lateral visual center, primarily involved in coordinating eye muscle movements and synergistic motions of the head and neck muscles related to ocular processes. The middle temporal gyrus plays a key role in integrating categorical characteristics into auditory and visual stimuli, while the occipital lobe serves as the core of the visual cortex, integral in the visual pathway, collectively constituting vital regions for vision-related functions. Previous research has indicated the presence

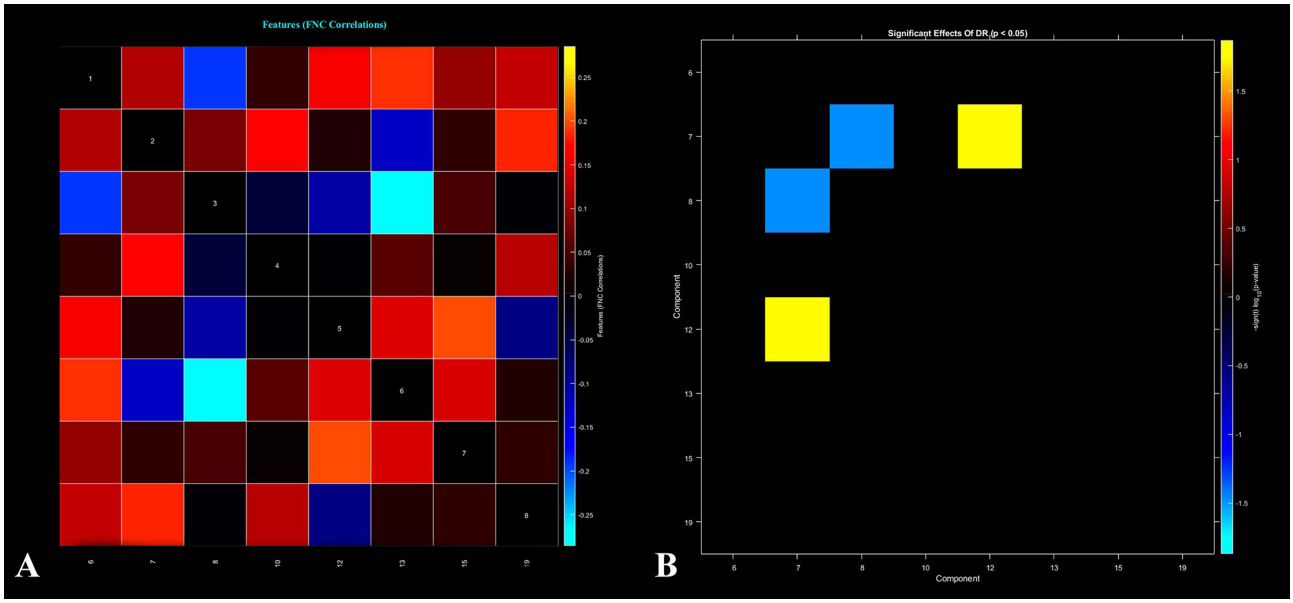

Figure 7 Functional connectivity matrix between all white matter networks (**A**), warm colors indicate positive correlations and cold colors indicate negative correlations. Differences in network functional connectivity between DR and HC groups (**B**) (p<0.05). DR, diabetic retinopathy; HC, healthy control.

Table 4 Different Internetwork FC Between the DR and HC

ICs	t-Values	p-Values
IC07-IC08	−2.1485	0.0344
IC07-IC12	2.5189	0.0135

Notes: The statistical threshold was set at the voxel level with $p < 0.05$ for multiple comparisons using Gaussian random-field theory. T-score represents the statistical value of peak voxel showing the differences in FC between the two groups.

Abbreviations: DR, diabetic retinopathy; HC, healthy control; IC, independent component; FC, functional connectivity.

of abnormal dynamic amplitude of low-frequency fluctuation (dALFF) activity in the middle frontal gyrus of individuals with diabetes and optic neuropathy.[46] Patients diagnosed with latent autoimmune diabetes in adults (LADA) exhibit abnormalities in the right occipital and temporal lobes.[47] Hence, we postulated that impairment in visually pertinent areas may contribute to the atypical manifestations observed in the middle cerebellar peduncle (MCP) among patients with DR.

The corpus callosum (CC) is the brain's largest bundle of interconnecting fibers, situated at the base of the longitudinal fissure. It comprises broad white matter, consisting of transverse fibers that facilitate communication between the right and left cerebral hemispheres.[48–50] The genu of the corpus callosum (GCC) is positioned in the anterior aspect of this structure, with fibers traversing this area curving forward into the frontal lobes bilaterally. Research investigating demyelination of the GCC region in mice revealed the essential involvement of interhemispheric communication between the frontal cortices in the top-down regulation of sensorimotor gating.[51] In a separate study involving children with type 1 diabetes mellitus, researchers identified an abnormal elevation in the apparent diffusion coefficient (ADC) within the genu of the corpus callosum (GCC). This anomaly was linked to early signs of myelinated fiber injury or axonal degeneration, potentially indicative of underlying neurological alterations.[52] In our study, patients with diabetic retinopathy (DR) exhibited an elevated degree centrality (DC) in the genu of the corpus callosum (GCC), suggesting a possible link to demyelinating lesions in the area and aberrant sensory-motor function.

The corona radiata (CR) comprises radially distributed fiber bundles that extend from the internal capsule to various inter-cortical regions of the brain, encompassing diverse white matter tracts. It is implicated in several psychiatric disorders, including attention-deficit hyperactivity disorder,[53] depression after total sleep deprivation,[54] and idiopathic clonic seizures.[55] The corona radiata exhibits diverse structural and functional changes in white matter integrity. A study involving diabetic individuals revealed that those with type 2 diabetes mellitus alongside peripheral microvascular complications displayed diminished fractional anisotropy (FA) and mean diffusivity (MD) values specifically in the bilateral superior corona radiata (SCR).[56] In our study, individuals with diabetic retinopathy (DR) exhibited significant abnormalities in the fractional amplitude of low-frequency fluctuation (fALFF) values within the region of the superior corona radiata (SCR). The precise mechanism behind this elevation remains ambiguous, likely owing to the intricate fiber arrangement within the corona radiata. Our hypothesis suggests that these changes may be associated with extensive structural and functional white matter alterations in DR patients, potentially contributing to underlying cognitive abnormalities.

The superior longitudinal fasciculus (SLF) is a major tract that connects extensive areas of the frontal and parietal lobes, comprising four subgroups: SLF I, SLF II, SLF III, and SLF IV.[57] Specifically, SLF II emerges from the angular gyrus and projects to the caudolateral prefrontal region, crucial for verbal, syntactic, and visuospatial processing.[58] This pathway contributes to modulating visuospatial attention effectively and is implicated in visuospatial ability,[59] and working memory in healthy adults.[60] Microstructural changes in the SLF influence visual perception significantly.[61] We postulate that patients with diabetic retinopathy (DR) may exhibit functional variations in visual processing regions, possibly leading to elevated fractional amplitude of low-frequency fluctuation (fALFF) values within the SLF.[56,62] Furthermore, individuals with type 2 diabetes mellitus and microangiopathy demonstrated decreased fractional anisotropy (FA) and mean diffusivity (MD) values in the right SLF. Another study examining white matter structure in type 2 diabetes mellitus patients highlighted alterations in various fiber tracts, including the SLF, the superior corona radiata

(SCR), and the posterior thalamic radiations (PTRs). Therefore, structural changes within the white matter of the SLF could contribute to the reduced fALFF values detected in the same region of DR patients.

The posterior thalamic radiation (PTR) serves as a pathway projecting to the cerebral cortex, including the optic radiation from the lateral geniculate body, through the posterior segment of the internal capsule, connecting the caudal-lateral thalamic nuclei to the posterior parietal and occipital lobes. Research has linked the function of the PTR to cognitive disorders such as schizophrenia[63–65] and Alzheimer's disease.[66] The PTR has been found to be functionally and structurally altered to varying degrees in a variety of studies on type 2 diabetes. For example, Sun et al found that FA values of the left PTR were reduced in type 2 diabetic patients without mild cognitive impairment[67] and Zhuo et al found that FA and MD values of the bilateral PTR were reduced in type 2 diabetic patients with microvascular complications.[56] In our investigation, we postulate that the reduced regional homogeneity (ReHo) values in the PTR of DR patients may be associated with cognitive deficits as well as white matter presence and possible structural changes in the white matter itself.

The uncinate fasciculus (UF) serves as a crucial pathway connecting the frontal and temporal lobes, vital for visceral emotional responses and semantic processing. Conditions involving emotion dysregulation, such as bi-directional affective disorder[68] and depression,[69,70] often manifest fiber structure irregularities in the UF. Similar findings are noted in studies on type 2 diabetes. Nouwen et al found that type 2 diabetes in adolescents was associated with significant changes in the FA of the left UF.[71] Qi et al found that bilateral UF integrity was reduced in elderly patients with type 2 diabetes with mild cognitive impairment.[72] Zhang et al similarly found that in type 2 diabetic patients with a left UF the generalized fractional anisotropy (GFA) values were significantly reduced.[69] Our current research suggests abnormal connection strengths between the UF and the posterior thalamic radiation (PTR) and anterior corona radiata (ACR) in diabetic retinopathy (DR) patients, inferring potential impairment in emotion regulation and cognitive function.

In our investigation, the intra-network anomalies revealed in diabetic retinopathy (DR) patients through Independent Component Analysis (ICA) closely correlated with abnormalities identified in degree centrality (DC), fractional amplitude of low-frequency fluctuations (fALFF), and Regional Homogeneity (ReHo) values obtained using BOLD-fMRI. Remarkably, these aberrant regions mirrored those documented in prior studies highlighting white matter structural irregularities in individuals with diabetes. For instance, Huang et al conducted a meta-analysis of diffusion tensor imaging (DTI) outcomes in type 2 diabetes mellitus, consistently unveiling reduced fractional anisotropy (FA) in the genu and body of the corpus callosum (GCC, BCC), as well as the bilateral anterior and superior corona radiata (ACR, SCR).[73] Zhuo et al found that patients with type 2 diabetes mellitus combined with microangiopathy had reduced FA values in CC, bilateral PTR, right SLF, and bilateral SCR and MD values were reduced;[56] Gao et al found that most of the WM changes in type 2 diabetes were located in the CC, CR, PTR, SLF, and UF.[62] We proposed that alterations in these regions observed in patients with DR may be more closely associated with elevated blood glucose levels. Additionally, as most of these regions are linked to visual and sensorimotor networks, impaired visual and sensorimotor functions in DR patients could also contribute to the irregularities found in these regions.

Support Vector Machine is a machine classification technique that has been used in a wide range of diseases.[74–76] The use of artificial intelligence to help doctors manage patients and aid in the diagnosis of diseases is growing everywhere, as the artificial intelligence integrate into our lives gradually. In this study, the accuracy of WM DC values, WM fALFF values and WM ReHo values as a feature to distinguish DR patients and HCs was 81.52%, 80.43% and 89.13%. And the ROC curve of the SVM classifier with an AUC value of 0.87, 0.85 and 0.93. These higher accuracies suggest that WM DC values, WM fALFF values and WM ReHo values can be used effectively as indicators to differentiate DR patients from HC patients.

Limitation

This is the inaugural article concerning the white matter capabilities and networking of individuals with diabetic retinopathy (DR); however, inherent limitations exist. Firstly, the relatively small sample size of DR patients may not adequately represent the actual scenario, thus posing limitations. Additionally, the unclear criteria for determining the number of components in ICA could impact the outcomes, with the optimal number possibly varying based on the context. Furthermore, manual identification of the white matter functional structure in the JHU atlas, as utilized in this study, introduces potential errors signaling the need for refining assessment algorithms in future research. Finally, This

study primarily investigates white matter functional alterations in diabetic retinopathy. Patients with diabetes without diabetic retinopathy were not included, despite sharing similar abnormal areas with previous white matter structural changes seen in diabetic patients. Future research will further explore and compare abnormal changes in brain white matter function and networks among diabetic retinopathy and type 2 diabetes patients.

Conclusion

The current study revealed significant white matter functional and network disruptions in DR patients, potentially originating from microstructural irregularities in white matter and abnormalities in grey matter structure and function. These alterations predominantly affected fiber tracts connecting the visual network to the sensory-motor network in DR patients, offering a novel perspective for exploring potential neurological irregularities in this patient population in future investigations.

Data Sharing Statement

The raw data supporting the conclusions of this article will be made available. Further inquiries can be directly to the corresponding author.

Acknowledgments

We acknowledge the assistance provided by the Natural Science Foundation of Jiangxi Province (20212BAB216058), Jiangxi Provincial Health Technology Project (202210012, 202310114 and 202410008), and Jiangxi Provincial traditional Chinese Technology Project (2022B840 and 2023A0138).

Disclosure

The authors declare that they have no conflict of interest in this work.

References

1. Antonetti DA, Klein R, Gardner TW. Diabetic Retinopathy. *N Engl J Med*. 2012;366:1227–1239. doi:10.1056/NEJMra1005073
2. Kollias AN, Ulbig MW. Diabetic Retinopathy. *Dtsch Arztebl Int*. 2010;107:75–84. doi:10.3238/arztebl.2010.0075
3. Teo ZL, Tham Y-C, Yu M, et al. Global prevalence of diabetic retinopathy and projection of burden through 2045: systematic review and meta-analysis. *Ophthalmology*. 2021;128(11):1580–1591. doi:10.1016/j.ophtha.2021.04.027
4. Tan T-E, Wong TY. Diabetic retinopathy: looking forward to 2030. *Front Endocrinol*. 2022;13:1077669. doi:10.3389/fendo.2022.1077669
5. Chai Y-H, Zhang Y-P, Qiao Y-S, et al. Association between diabetic retinopathy, brain structural abnormalities, and cognitive impairment for accumulated evidence in observational studies. *Am J Ophthalmol*. 2022;239:37–53. doi:10.1016/j.ajo.2022.01.011
6. Chai Y-H, Han Y-P, Zhang J-Y, Zhou J-B. Diabetic retinopathy and brain structure, cognition function, and dementia: a bidirectional Mendelian randomization study. *J Alzheimers Dis*. 2024;97:1211–1221. doi:10.3233/JAD-231022
7. Little,K, Llorián-Salvador M, Scullion S, et al. Common pathways in dementia and diabetic retinopathy: understanding the mechanisms of diabetes-related cognitive decline. *Trends Endocrinol Metab*. 2022;33(1):50–71. doi:10.1016/j.tem.2021.10.008
8. Mills SA, Jobling AI, Dixon MA, et al. Fractalkine-induced microglial vasoregulation occurs within the retina and is altered early in diabetic retinopathy. *Proc Natl Acad Sci U S A*. 2021;118:e2112561118. doi:10.1073/pnas.2112561118
9. Huang Y, Wang S, Cai C, et al. Retinal vascular density as a potential biomarker of diabetic cerebral small vessel disease. *Diabetes Obes Metab*. 2024;26(5):1789–1798. doi:10.1111/dom.15492
10. Fang F, Zhan Y-F, Zhuo -Y-Y, et al. Brain atrophy in middle-aged subjects with Type 2 diabetes mellitus, with and without microvascular complications. *J Diabetes*. 2018;10:625–632. doi:10.1111/1753-0407.12646
11. van Duinkerken E, Steenwijk MD, Klein M, et al. Accelerated executive functions decline and gray matter structural changes in middle-aged type 1 diabetes mellitus patients with proliferative retinopathy. *J Diabetes*. 2018;10:835–846. doi:10.1111/1753-0407.12773
12. Wessels AM, Simsek S, Remijnse PL, et al. Voxel-based morphometry demonstrates reduced grey matter density on brain MRI in patients with diabetic retinopathy. *Diabetologia*. 2006;49:2474–2480. doi:10.1007/s00125-006-0283-7
13. Hansen TM, Muthulingam JA, Brock B, et al. Reduced gray matter brain volume and cortical thickness in adults with type 1 diabetes and neuropathy. *Neurosci Res*. 2022;176:66–72. doi:10.1016/j.neures.2021.10.002
14. Burgess J, de Bezenac C, Keller SS, et al. Brain alterations in regions associated with end-organ diabetic microvascular disease in diabetes mellitus: a UK biobank study. *Diabetes Metab Res Rev*. 2024;40(2):e3772. doi:10.1002/dmrr.3772
15. Ferreira FS, Pereira JMS, Reis A, et al. Early visual cortical structural changes in diabetic patients without diabetic retinopathy. *Graefes Arch Clin Exp Ophthalmol*. 2017;255(11):2113–2118. doi:10.1007/s00417-017-3752-4
16. Hugenschmidt CE, Lovato JF, Ambrosius WT, et al. The cross-sectional and longitudinal associations of diabetic retinopathy with cognitive function and brain MRI findings: the action to control cardiovascular risk in diabetes (ACCORD) trial. *Diabetes Care*. 2014;37(12):3244–3252. doi:10.2337/dc14-0502

17. Qi C-X, Huang X, Shen Y. Altered intrinsic brain activities in patients with diabetic retinopathy using amplitude of low-frequency fluctuation: a resting-state fMRI study. *Diabetes Metab Syndr Obes*. 2020;13:2833–2842. doi:10.2147/DMSO.S259476
18. Wang Z-L, Zou L, Lu Z-W, et al. Abnormal spontaneous brain activity in type 2 diabetic retinopathy revealed by amplitude of low-frequency fluctuations: a resting-state fMRI study. *Clin Radiol*. 2017;72:340.e1–340.e7. doi:10.1016/j.crad.2016.11.012
19. Shi W-Q, Zhang M-X, Tang L-Y, et al. Altered spontaneous brain activity patterns in patients with diabetic retinopathy using amplitude of low-frequency fluctuation. *World J Diabetes*. 2022;13(2):97–109. doi:10.4239/wjd.v13.i2.97
20. Li L, Dai H, Ke J, et al. Resting-state functional MRI study: connection strength of brain networks in DR patients. *NDT*. 2019;15:3359–3366. doi:10.2147/NDT.S227468
21. Wang Y, Jiang L, Wang X-Y, et al. Evidence of altered brain network centrality in patients with diabetic nephropathy and retinopathy: an fMRI study using a voxel-wise degree centrality approach. *Ther Adv Endocrinol Metab*. 2019;10:2042018819865723. doi:10.1177/2042018819865723
22. Liao X-L, Yuan Q, Shi W-Q, et al. Altered brain activity in patients with diabetic retinopathy using regional homogeneity: a Resting-State fMRI study. *Endocr Pract*. 2019;25(4):320–327. doi:10.4158/EP-2018-0517
23. Huang Y, Bailey SK, Wang P, et al. Voxel-wise detection of functional networks in white matter. *NeuroImage*. 2018;183:544–552. doi:10.1016/j.neuroimage.2018.08.049
24. Li J, Biswal BB, Wang P, et al. Exploring the functional connectome in white matter. Human brain mapping. 2019;40(15):4331–44. doi:10.1002/hbm.24705
25. Peer M, Nitzan M, Bick AS, Levin N, Arzy S. Evidence for functional networks within the human brain's white matter. *J Neurosci*. 2017;37:6394–6407. doi:10.1523/JNEUROSCI.3872-16.2017
26. Lama RK, Lee S-W. White matter network alterations in alzheimer's disease patients. *Appl Sci*. 2020;10:919. doi:10.3390/app10030919
27. Meng L, Wang H, Zou T, et al. Attenuated brain white matter functional network interactions in Parkinson's disease. *Human Brain Mapp*. 2022;43:4567–4579. doi:10.1002/hbm.25973
28. Zhou Z, Qian L, Xu J, et al. Topologic reorganization of white matter connectivity networks in early-blind adolescents. *Neural Plast*. 2022;2022:1–11. doi:10.1155/2022/8034757
29. Muthulingam JA, Brock C, Hansen TM, et al. Disrupted white matter integrity in the brain of type 1 diabetes is associated with peripheral neuropathy and abnormal brain metabolites. *J Diabetes Complicat*. 2022;36(9):108267. doi:10.1016/j.jdiacomp.2022.108267
30. Ling M, Zhou J, Pang X-Q, et al. White matter microstructural abnormalities of the visual pathway in type 2 diabetes mellitus: a generalized Q-sampling imaging study. *Acad Radiol*. 2022;29 Suppl 3:S166–S174. doi:10.1016/j.acra.2021.10.021
31. Xiao A, Ge Q-M, Zhong H-F, et al. White matter hyperintensities of bilateral lenticular putamen in patients with proliferative diabetic retinopathy: a voxel-based morphometric study. *Diabetes Metab Syndr Obes*. 2021;14:3653–3665. doi:10.2147/DMSO.S321270
32. Wu G-R, Stramaglia S, Chen H, Liao W, Marinazzo D. Mapping the voxel-wise effective connectome in resting state fMRI. *PLoS One*. 2013;8:e73670. doi:10.1371/journal.pone.0073670
33. Yan C-G, Cheung B, Kelly C, et al. A comprehensive assessment of regional variation in the impact of head micromovements on functional connectomics. *Neuroimage*. 2013;76:183–201. doi:10.1016/j.neuroimage.2013.03.004
34. Zou Q-H, Zhu C-Z, Yang Y, et al. An improved approach to detection of amplitude of low-frequency fluctuation (ALFF) for resting-state fMRI: fractional ALFF. *J Neurosci Methods*. 2008;172(1):137–141. doi:10.1016/j.jneumeth.2008.04.012
35. Zuo X-N, Di Martino A, Kelly C, et al. The oscillating brain: complex and reliable. *Neuroimage*. 2010;49(2):1432–1445. doi:10.1016/j.neuroimage.2009.09.037
36. Zang Y, Jiang T, Lu Y, He Y, Tian L. Regional homogeneity approach to fMRI data analysis. *NeuroImage*. 2004;22:394–400. doi:10.1016/j.neuroimage.2003.12.030
37. Tononi G, McIntosh AR, Russell DP, Edelman GM. Functional clustering: identifying strongly interactive brain regions in neuroimaging data. *NeuroImage*. 1998;7:133–149. doi:10.1006/nimg.1997.0313
38. Smitha KA, Arun KM, Rajesh PG, et al. Resting fMRI as an alternative for task-based fMRI for language lateralization in temporal lobe epilepsy patients: a study using independent component analysis. *Neuroradiology*. 2019;61(7):803–810. doi:10.1007/s00234-019-02209-w
39. Xing -X-X, Hua X-Y, Zheng M-X, et al. High-order brain networks abnormalities in osteonecrosis of the femoral head patients: an independent component analysis of resting-state fMRI. *Pain Physician*. 2022;25:E1475–E1484.
40. Kumar U, Arya A, Agarwal V. Neural network connectivity in ADHD children: an independent component and functional connectivity analysis of resting state fMRI data. *Brain Imaging Behav*. 2021;15:157–165. doi:10.1007/s11682-019-00242-0
41. Schrouff J, Rosa MJ, Rondina JM, et al. PRoNTo: pattern recognition for neuroimaging toolbox. *Neuroinformatics*. 2013;11(3):319–337. doi:10.1007/s12021-013-9178-1
42. Huang Y, Yang Y, Hao L, et al. Detection of functional networks within white matter using independent component analysis. *NeuroImage*. 2020;222:117278. doi:10.1016/j.neuroimage.2020.117278
43. Wakana S, Caprihan A, Panzenboeck MM, et al. Reproducibility of quantitative tractography methods applied to cerebral white matter. *NeuroImage*. 2007;36(3):630–644. doi:10.1016/j.neuroimage.2007.02.049
44. Hua K, Zhang J, Wakana S, et al. Tract probability maps in stereotaxic spaces: analyses of white matter anatomy and tract-specific quantification. *NeuroImage*. 2008;39(1):336–347. doi:10.1016/j.neuroimage.2007.07.053
45. Andica C, Kamagata K, Uchida W, et al. White matter fiber-specific degeneration in older adults with metabolic syndrome. *Mol Metabol*. 2022;62: 101527.
46. Yang L, Xiao A, Li Q-Y, et al. Hyperintensities of middle frontal gyrus in patients with diabetic optic neuropathy: a dynamic amplitude of low-frequency fluctuation study. *Aging*. 2022;14(3):1336–1350. doi:10.18632/aging.203877
47. Miao Y, Wang J, Zhang B, et al. Altered brain spontaneous and synchronization activity in latent autoimmune diabetes in adults: a resting-state functional MRI study. *Diabetes Metab Res Rev*. 2023;39(1):e3587. doi:10.1002/dmrr.3587
48. Bloom JS, Hynd GW. The role of the corpus callosum in interhemispheric transfer of information: excitation or inhibition? *Neuropsychol Rev*. 2005;15:59–71. doi:10.1007/s11065-005-6252-y
49. Caillé S, Sauerwein HC, Schiavetto A, Villemure J-G, Lassonde M. Sensory and motor interhemispheric integration after section of different portions of the anterior corpus callosum in nonepileptic patients. *Neurosurgery*. 2005;57(1):50–59. doi:10.1227/01.NEU.0000163089.31657.08
50. Roland JL, Snyder AZ, Hacker CD, et al. On the role of the corpus callosum in interhemispheric functional connectivity in humans. *Proc Natl Acad Sci USA*. 2017;114:13278–13283. doi:10.1073/pnas.1707050114

51. Xiao G, Li H, Hu X, et al. Interference of commissural connections through the genu of the corpus callosum specifically impairs sensorimotor gating. *Behav Brain Res*. 2021;411:113383. doi:10.1016/j.bbr.2021.113383
52. Toprak H, Yetis H, Alkan A, et al. Relationships of DTI findings with neurocognitive dysfunction in children with Type 1 diabetes mellitus. *Br J Radiol*. 2016;89(1059):20150680. doi:10.1259/bjr.20150680
53. Wang L-J, Li S-C, Chou W-J, et al. Human transcriptome array analysis and diffusion tensor imaging in attention-deficit/hyperactivity disorder. *J Psychiatr Res*. 2024;172:229–235. doi:10.1016/j.jpsychires.2024.02.047
54. Taraku B, Zavaliangos-Petropulu A, Loureiro JR, et al. White matter microstructural perturbations after total sleep deprivation in depression. *Front Psychiatry*. 2023;14:1195763. doi:10.3389/fpsyt.2023.1195763
55. Liu G, Lyu G, Yang N, et al. Abnormalities of diffusional kurtosis imaging and regional homogeneity in idiopathic generalized epilepsy with generalized tonic-clonic seizures. *Exp Ther Med*. 2018. doi:10.3892/etm.2018.7018
56. Zhuo Y, Fang F, Lu L, et al. White matter impairment in type 2 diabetes mellitus with and without microvascular disease. *Neuroimage Clin*. 2019;24:101945. doi:10.1016/j.nicl.2019.101945
57. Makris N, Kennedy DN, McInerney S, et al. Segmentation of subcomponents within the superior longitudinal fascicle in humans: a quantitative, in vivo, DT-MRI study. *Cereb Cortex*. 2005;15(6):854–869. doi:10.1093/cercor/bhh186
58. De Schotten MT, Dell'Acqua F, Forkel SJ, et al. A lateralized brain network for visuospatial attention. *Nat Neurosci*. 2011;14(10):1245–1246. doi:10.1038/nn.2905
59. Hong X, Zheng L, Rajan A, Ding M. Role of superior longitudinal fasciculus in visual spatial attention. *J Vis*. 2019;19:320.
60. Koshiyama D, Fukunaga M, Okada N, et al. Association between the superior longitudinal fasciculus and perceptual organization and working memory: a diffusion tensor imaging study. *Neurosci Lett*. 2020;738:135349. doi:10.1016/j.neulet.2020.135349
61. Kim S-H, Jeon H-E, Park C-H. Relationship between visual perception and microstructural change of the superior longitudinal fasciculus in patients with brain injury in the right hemisphere: a preliminary diffusion tensor tractography study. *Diagnostics*. 2020;10:641. doi:10.3390/diagnostics10090641
62. Gao J, Pan P, Li J, et al. Analysis of white matter tract integrity using diffusion kurtosis imaging reveals the correlation of white matter microstructural abnormalities with cognitive impairment in type 2 diabetes mellitus. *Front Endocrinol*. 2024;15: 1327339.
63. Wu X, Kang X-W, Li X, et al. Baseline white matter function predicts short-term treatment response in first-episode schizophrenia. *J Neuroimaging*. 2023;33:632–643. doi:10.1111/jon.13101
64. Meng L, Li K, Li W, et al. Widespread white-matter microstructure integrity reduction in first-episode schizophrenia patients after acute antipsychotic treatment. *Schizophr Res*. 2019;204:238–244. doi:10.1016/j.schres.2018.08.021
65. Tan AS, Chew QH, Sim K. Cerebral white matter changes in deficit and non-deficit subtypes of schizophrenia. *J Neural Transm*. 2020;127:1073–1079. doi:10.1007/s00702-020-02207-w
66. Huang C-W, Tsai M-H, Chen N-C, et al. Clinical significance of circulating vascular cell adhesion molecule-1 to white matter disintegrity in Alzheimer's dementia. *Thromb Haemostasis*. 2015;114(12):1230–1240. doi:10.1160/TH14-11-0938
67. Sun Q, Chen G-Q, Wang X-B, et al. Alterations of white matter integrity and hippocampal functional connectivity in type 2 diabetes without mild cognitive impairment. *Front Neuroanat*. 2018;12(21). doi:10.3389/fnana.2018.00021.
68. Xu E, Nguyen L, Hu R, et al. The uncinate fasciculus in individuals with and at risk for bipolar disorder: a meta-analysis. *J Affective Disorders*. 2022;297:208–216. doi:10.1016/j.jad.2021.10.045
69. Zhang A, Leow A, Ajilore O, et al. Quantitative tract-specific measures of uncinate and cingulum in major depression using diffusion tensor imaging. *Neuropsychopharmacology*. 2012;37:959–967. doi:10.1038/npp.2011.279
70. Xu EP, Nguyen L, Leibenluft E, Stange JP, Linke JO. A meta-analysis on the uncinate fasciculus in depression. *Psychol Med*. 2023;53:2721–2731. doi:10.1017/S0033291723000107
71. Nouwen A, Chambers A, Chechlacz M, et al. Microstructural abnormalities in white and gray matter in obese adolescents with and without type 2 diabetes. *Neuroimage Clin*. 2017;16:43–51. doi:10.1016/j.nicl.2017.07.004
72. Qi D, Wang A, Chen Y, et al. Default mode network connectivity and related white matter disruption in type 2 diabetes mellitus patients concurrent with amnestic mild cognitive impairment. *Curr Alzheimer Res*. 2017;14(11):1238–1246. doi:10.2174/1567205014666170417113441
73. Huang L, Zhang Q, Tang T, et al. Abnormalities of brain white matter in type 2 diabetes mellitus: a meta-analysis of diffusion tensor imaging. *Front Aging Neurosci*. 2021;13:693890. doi:10.3389/fnagi.2021.693890
74. He D, Ren D, Guo Z, Jiang B. Insomnia disorder diagnosed by resting-state fMRI-based SVM classifier. *Sleep Med*. 2022;95:126–129. doi:10.1016/j.sleep.2022.04.024
75. Ibrahim B, Suppiah S, Ibrahim N, et al. Diagnostic power of resting-state fMRI for detection of network connectivity in Alzheimer's disease and mild cognitive impairment: a systematic review. *Hum Brain Mapp*. 2021;42:2941–2968. doi:10.1002/hbm.25369
76. Santana CP, de Carvalho EA, Rodrigues ID, et al. rs-fMRI and machine learning for ASD diagnosis: a systematic review and meta-analysis. *Sci Rep*. 2022;12(1):6030. doi:10.1038/s41598-022-09821-6